Stochastic simulation model for nonstationary time series using an autoregressive wavelet decomposition: Applications to rainfall and temperature

Hyun-Han Kwon,[1] Upmanu Lall,[1] and Abedalrazq F. Khalil[1]

Received 19 June 2006; revised 2 February 2007; accepted 15 February 2007; published 2 May 2007.

[1] A time series simulation scheme based on wavelet decomposition coupled to an autoregressive model is presented for hydroclimatic series that exhibit band-limited low-frequency variability. Many nonlinear dynamical systems generate time series that appear to have amplitude- and frequency-modulated oscillations that may correspond to the recurrence of different solution regimes. The use of wavelet decomposition followed by an autoregressive model of each leading component is explored as a model for such time series. The first example considered is the Lorenz-84 low-order model of extratropical circulation, which has been used to illustrate how chaos and intransitivity (multiple stable solutions) can lead to low-frequency variability. The central England temperature (CET) time series, the NINO3.4 series that is a surrogate for El Nino–Southern Oscillation, and seasonal rainfall from Everglades National Park, Florida, are then modeled with this approach. The proposed simulation model yields better results than a traditional linear autoregressive (AR) time series model in terms of reproducing the time-frequency properties of the observed rainfall, while preserving the statistics usually reproduced by the AR models.

Citation: Kwon, H.-H., U. Lall, and A. F. Khalil (2007), Stochastic simulation model for nonstationary time series using an autoregressive wavelet decomposition: Applications to rainfall and temperature, *Water Resour. Res.*, *43*, W05407, doi:10.1029/2006WR005258.

1. Introduction

[2] Stochastic hydrologic methods have been very useful for a variety of water resources problems where temporal uncertainty needs to be quantified. The time series models that were developed extensively since the 1960s have typically assumed that the series modeled comes from a stationary or cyclostationary process. Thus the literature [*Box and Jenkins*, 1970; *Thomas and Fiering*, 1962; *Yevjevich*, 1972] has developed around autoregressive moving average models and their extensions to consider seasonality through periodic terms. Multisite models and space-time disaggregation approaches have also been considered [*Koutsoyiannis*, 1994; *Stedinger and Vogel*, 1984; *Valencia and Schaake*, 1973].

[3] However, as record lengths have increased, hydrologists have become aware of the low-frequency structure (e.g., oscillations such ENSO, PDO, NAO) of climate and associated hydrologic time series [*Dettinger et al.*, 1995; *Ghil and Vautard*, 1991; *Keppenne and Ghil*, 1992a; *Keppenne and Lall*, 1996; *Lall and Mann*, 1995; *Mann and Park*, 1993, 1994, 1996]. Traditionally, an ARMA (p, q) model is considered for such a time series. Such a model is capable of generating linear oscillations, even with relatively low values of p and q. However, applications of such models often do not reproduce the spectral signature of the time series, specifically the amplitude-frequency modulation over time that is seen in moving window spectra or wavelet spectra. Such temporal variations could be generated by (1) nonlinear autoregressive models [e.g., *Tong*, 1990], (2) time varying AR [e.g., *Huang and Chalabi*, 1995], (3) autoregressive conditionally heteroscedastic (ARCH) models [e.g., *Ahn and Kim*, 2005], (4) nonparametric approximations to nonlinear autoregressive models [e.g., *Lall and Sharma*, 1996], (5) hidden Markov models [e.g., *Hughes and Guttorp*, 1999; *Robertson et al.*, 2004], and (6) empirical decompositions of the low-frequency signals and noise using spectral methods followed by linear autoregressive models [e.g., *Jiang et al.*, 1995; *Keppenne and Ghil*, 1992a, 1992b]. The idea of decomposing the time series into components that correspond to simpler dynamical systems with characteristic dynamics at particular scales is pragmatically attractive, even though a low-order nonlinear autoregressive model [e.g., *Abarbanel*, 1996; *Abarbanel and Lall*, 1996] that automatically simulates the desired behavior may be more intellectually satisfying. A multitaper (MTM) based approach along with AR modeling in a forecasting context was developed by *Rajagopalan et al.* [1998].

[4] An objective of this study is to explore the use of autoregressive models with wavelet decomposition as a time series simulator for systems with (1) quasiperiodic long memory behavior or (2) nonlinear dynamics that may lead to persistent regime like behavior or (3) stochastic

[1]Department of Earth and Environmental Engineering, Columbia University, New York, New York, USA.

0043-1397/07/2006WR005258$09.00

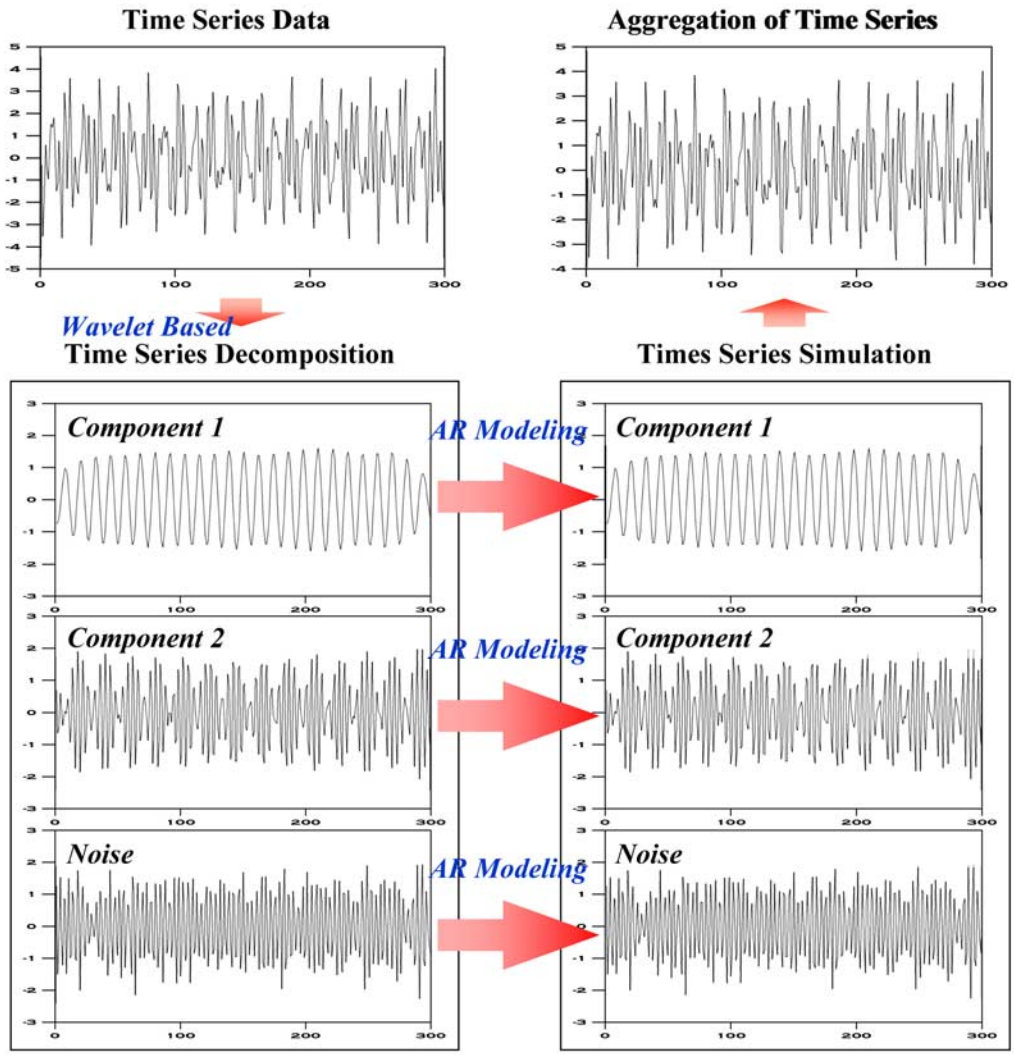

Figure 1. WARM simulation procedure. The time series is decomposed using a continuous wavelet transform using the Morlet wavelet basis, and the components whose global wavelet power exceeds the 95% of the spectrum associated with a red noise background are retained. Optimum lag orders of each dominant component are estimated by the Akaike information criteria, and autoregression parameters are estimated via maximum likelihood under the assumption that the residuals are normally distributed.

regime transitions, without a priori specifying any of these modeling structures. The continuous wavelet transform is applied to decompose a univariate time series into several statistically significant components and then a linear AR model is employed to simulate each component extracted from wavelet transform analysis, as well as the residual "noise" term. The intent of this study was exploratory procedures; to attain the best possible fit to a data set were not an explicit goal.

[5] The general approach is described in the next section. Four applications follow. The first considers time series data from a deterministic, numerical model that provides some motivation for the physical context of the problem. The next three test the approach with some relatively long hydroclimatic time series where the ability to reproduce interannual variability may be of interest. A discussion of the applicability of the method and of potential future directions concludes the paper.

2. Wavelet Autoregressive Model

[6] Consider a time series x_t, $t = 1,\ldots, N$, recorded at monthly intervals, that exhibits quasi-oscillatory, low-frequency variations at intraseasonal, interannual and longer timescales, as seen in many hydroclimatic time series. Consider the decomposition (see Figure 1) of this series into K component series R_{kt} that represent "signal" and a residual term ε_t.

$$x_t = \sum_{k=1}^{K} R_{kt} + \varepsilon_t \tag{1}$$

[7] The decomposition in (1) considers that there are K orthogonal or independent series that carry the low-frequency

information, and the residual, ε_t, is a stochastic process. The notion is that the dynamics of each of these terms (R_{kt} and ε_t) is simpler to model using an autoregressive model than an autoregressive model for the composite dynamics of all the components. In general, each could be modeled using an appropriate time series technique (e.g., linear of nonlinear). Here we consider a linear autoregressive model for each term, leading to the following model structure:

$$x_t = \sum_{k=1}^{K} AR(R_{kt}; p_k) + AR(\varepsilon_t; p)$$

$$= \sum_{k=1}^{K} \left(\sum_{i=1}^{p_k} \alpha_{k,i} R_{t-i,k} + v_{t,k} \right) + \sum_{j=1}^{p} \beta_j \varepsilon_{t-j} + \omega_t \quad (2)$$

[8] Here p_k is the order of an autoregressive model fit to the kth signal, $\alpha_{k,i}$ are the corresponding autoregression coefficients; p is the order of an autoregressive model fit to the stochastic process ε_t, with β_j as the associated autoregression coefficients, and $v_{t,k}$ and ω_t are independent, identically distributed, noise processes. Note that this is a very simple additive model with no interactions across the noise or the signals. The question is whether such a model can capture the low- and high-frequency dynamics of hydroclimatic time series better than a traditional autoregressive model applied directly to the time series x_t. Noting that the order (p_k or p) of each autoregressive model and the coefficients of each autoregression in (2) can be estimated using standard time series methods (e.g., maximum likelihood and Akaike information criteria (AIC) [*Akaike*, 1974]), the procedures for the selection of the "signals" R_{kt} in the decomposition in equation (1) are described next.

2.1. Wavelet Transform for Time Series Decomposition

[9] The wavelet transform has been applied to many geophysical time series [e.g., *Farge*, 1992; *Foufoula-Georgiou and Kumar*, 1995; *Hubbard*, 1996; *Kulkarni*, 2000; *Torrence and Compo*, 1998; *Wang and Wang*, 1996; *Weng and Lau*, 1994]. The main advantage cited for wavelet transforms over other spectral methods is that they permit an orthogonal decomposition of the original signal in the time and in the frequency domain. This is an attractive property in the context of the additive decomposition suggested in equation (1). We briefly summarize the presentation of the wavelet transform by *Torrence and Compo* [1998] for our problem context.

[10] The term wavelets refers to sets of functions of the form $\varphi_{b,a}(t) = |a|^{-1/2}\varphi((t-b)/a)$, i.e., sets of functions formed by dilation and translation of a single function $\varphi(t)$, called the mother wavelet. The continuous wavelet transform of a real time series $x(t)$ is defined by [*Chui*, 1992]:

$$X(b,a) = |a|^{-1/2} \int_{-\infty}^{+\infty} x(t)\varphi^*((t-b)/a)dt \quad (3)$$

where $X(b, a)$ is a wavelet spectrum, $\varphi(t)$ is a wavelet function, the (*) indicates the complex conjugate, b is the translation (shift) parameter and $a \neq 0$ is the scale parameter. By localizing the wavelet function at $t - b = 0$ and then by computing the coefficients $X(b, a)$ we can explore the behavior of $x(t)$ near $t = b$. A variety of wavelet functions have been proposed [*Foufoula-Georgiou and Kumar*, 1995; *Torrence and Compo*, 1998]. Here we have used the Morlet wavelet, defined as $\varphi(t) = \pi^{-1/4} e^{i\omega_o t} e^{-t^2/2}$, where ω_0 is a frequency. To estimate the continuous wavelet transform, an N times convolution of function (1) is done for each scale, where N is the number of points in the time series [*Kaiser*, 1994]. Numerically, we are able to estimate the wavelet power spectrum in Fourier space, at N given points, using a discrete Fourier transform (x_n) as done by *Torrence and Compo* [1998].

$$\hat{x}_j = \frac{1}{N} \sum_{n=0}^{N-1} x_n \exp(-2\pi i j n/N) \quad (4)$$

where $j = 0, \ldots, N-1$ is the frequency index. In the continuous limit, the Fourier transform of a function $\varphi(t/a)$ is given by $\hat{\varphi}(a\omega)$. By the convolution theorem, the wavelet transform is the inverse Fourier transform of the product:

$$X_n(a) = \sum_{j=0}^{N-1} \hat{x}_j \hat{\varphi}^*(a\omega_j) \exp(i\omega_j n \delta_t) \quad (5)$$

[11] We can interpret the information in the wavelet power spectrum at each time and scale in two ways, as suggested by *Torrence and Compo* [1998]. One is the time-integrated variance of energy coefficients at every scale to construct the global wavelet power and another one is the scale-integrated variance of energy coefficients over time to compute the scale-averaged wavelet power (SAWP) as

[12] GWP

$$\bar{X}_n^2(a) = \frac{1}{N} \sum_{n=0}^{N-1} |X_n(a)|^2 \quad (6)$$

[13] SAWP

$$\bar{X}_n^2(t) = \frac{\delta_j \delta_t}{C_\delta} \sum_{j=j_1}^{j_2} \frac{|X_n(a_j)|^2}{a_j} \quad (7)$$

[14] The C_δ is a reconstruction coefficient and is a constant for each wavelet function; j_1 and j_2 are scales over which the averaging takes place; δ_j and δ_t are the scale averaging coefficient, sampling period respectively.

[15] The GWP for x_t is computed as a function of the scale a. A "red noise" significance test for the GWP(x) is then developed following the procedure described by *Torrence and Compo* [1998]. It entails first fitting an AR(1) model to x_t, and then computing its Fourier spectrum, and the associated one-sided 95% confidence limits as a function of frequency. The scales a_j for which the GWP(x) spectrum is higher than the red noise significance level are then selected as candidates for reconstruction. Conceptually, this decomposition is similar to what a Hidden Markov Model (HMM) may try to do. A HMM introduces latent variables that cluster the state-space in a way such that regime transitions from one state or cluster to another follow a Markov process. Given the transition probability matrix across such states, low-frequency, quasiperiodic behavior could be generated. The scale decomposition is explicit in the wavelet approach while it is implicit in the HMM.

[16] Following the reconstructed component series R_{kt} can be estimated by the sum of the real part of the wavelet transform over the scale associated with the kth component as

$$R_{kn} = \frac{\delta_k \delta_t^{1/2}}{C_\delta \psi_0(0)} \frac{\Re\{X_n(a_k)\}}{a_k^{1/2}} \tag{8}$$

[17] The factor ψ_0 (0) removes the energy scaling, while the $a_k^{1/2}$ converts the wavelet transform to an energy density. The factor C_δ comes from the reconstruction of a δ function from its wavelet transform using the wavelet function ψ_0 (η).

3. Applications

[18] Four applications are considered. First, a time series is selected from the 3 variable, seasonally forced [*Lorenz*, 1984] model of the interactions of the extratropical mean flow with the eddies. This is an interesting application because this set of ordinary differential equations is know to exhibit (1) chaos, or sensitive dependence on initial conditions, (2) intransitivity, or the presence of multiple stable solutions, and (3) organized, temporal variability that is internally generated by the feedbacks in the model, and reflects both the path dependence and the transitions to multiple stable solutions. The *Lorenz* [1984] model is a toy model that captures an important element of the quasi-geostrophic circulation of the atmosphere in the midlatitudes and its dependence on surface temperature gradients. It has been analyzed in the nonlinear state-space reconstruction literature [*Kennel et al.*, 1992; *Kennel and Mees*, 2000] and has also been used to understand seasonality [*Jain*, 1998] and responses of the circulation to slowly changing climate [*Jain et al.*, 1999; *Roebber*, 1995].

[19] Applications to three real world time series are also presented; the 346 year record of annual central England temperature, the 150 year record of the NINO3.4 index of ENSO, and the 36 year record of seasonal rainfall in the Everglades National Park.

3.1. Lorenz-84 Seasonal Model

[20] *Lorenz* [1984, 1990] proposed a simplified description of midlatitude atmosphere dynamics. The model equations are as follows:

$$\begin{aligned} \frac{dX}{dt} &= -Y^2 - Z^2 - aX + aF \\ \frac{dY}{dt} &= XY - bXZ - Y + G \\ \frac{dZ}{dt} &= bXY + XZ - Z \end{aligned} \tag{9}$$

[21] In these equations X represents the strength of the westerly flow, whose mean value is proportional to the average temperature gradient between equator and pole. The variables Y and Z are Fourier amplitudes characterizing a chain of large-scale eddies coupled to the mean flow. The term F and G represent equator to pole temperature gradient and ocean-land temperature contrast, respectively.

[22] Here we took $a = 0.25$, $b = 4$, and $\partial t = 5$days, $F = 7 + 2\cos(2\pi\ t/T)$ and $G = 1$, and sampled the X state variable with $\partial t = 5$ days.

[23] An AR model and a wavelet autoregressive model (WARM) model were fitted to this time series. Since the AR model is linear, we do not expect it to perform well in this nonlinear setting. The question is whether the WARM approach is effective, even though it uses linear AR models on component time series. In both cases, the AR model order was selected by AIC. The optimal order for the AR model was one. Seven components in the 10 to 30 day band were identified by the wavelet model applied to the Lorenz model time series. The optimal AIC order for these models and the residual noise term ranged from one to three. One thousand stochastic simulations each were then generated from the AR model and from the WARM model. In all cases, the residual noise processes were assumed to be normally distributed.

[24] The Lorenz-84 time series (Figure 2a), its Wavelet power spectrum and the corresponding global wavelet power spectrum of Lorenz-84 are shown in Figure 2b. Figure 3a shows the relative frequency of the numerically simulated Lorenz time series and for the corresponding average over the 1000 AR and the 1000 WARM simulations. We note a significant bias in the AR model's frequency distribution, as expected given that neither the nonlinearity in the dynamics, nor the marginal probability distribution were explicitly modeled. However, the WARM simulations do reproduce the marginal distribution on average, even though the components and the noise process are modeled in the same way as for the AR model.

[25] The temporal structure of the simulated time series is assessed using the global wavelet power spectrum (GWP). Figure 3b presents a comparison of GWP of the original numerical simulation and the averages with spectral uncertainties (5%, 95%) of the 1000 stochastic simulations using AR and WARM. The spectral signature of the original series is reproduced much better by the WARM simulations than by the AR simulations. Thus, in this case, WARM reproduces both the marginal distribution and the temporal frequency structure. These are aspects that are of primary interest for stochastic hydrology. The spectral uncertainties associated with the WARM simulation are relatively high as expected given the much lager number of parameters than with the AR model. The uncertainty band is much tighter around the mean AR spectrum, and the original spectral peak of interest is well outside that band.

[26] One could consider that since WARM was developed using wavelets, a comparison using a wavelet spectrum is biased in its favor. We note that the decomposition and the subsequent linear modeling approach do not automatically guarantee such an outcome since relatively ad hoc criteria are used for model selection and construction (e.g., linear, AIC, 95% red noise significance for choosing frequencies). Clearly, each component AR model has to be successful in reproducing the relevant aspects of each component. The mixing of these stochastically generated components is also not guaranteed to result in the right marginal distribution. Further, WARM reproduces the lower-frequency (32–1024 days) GWP

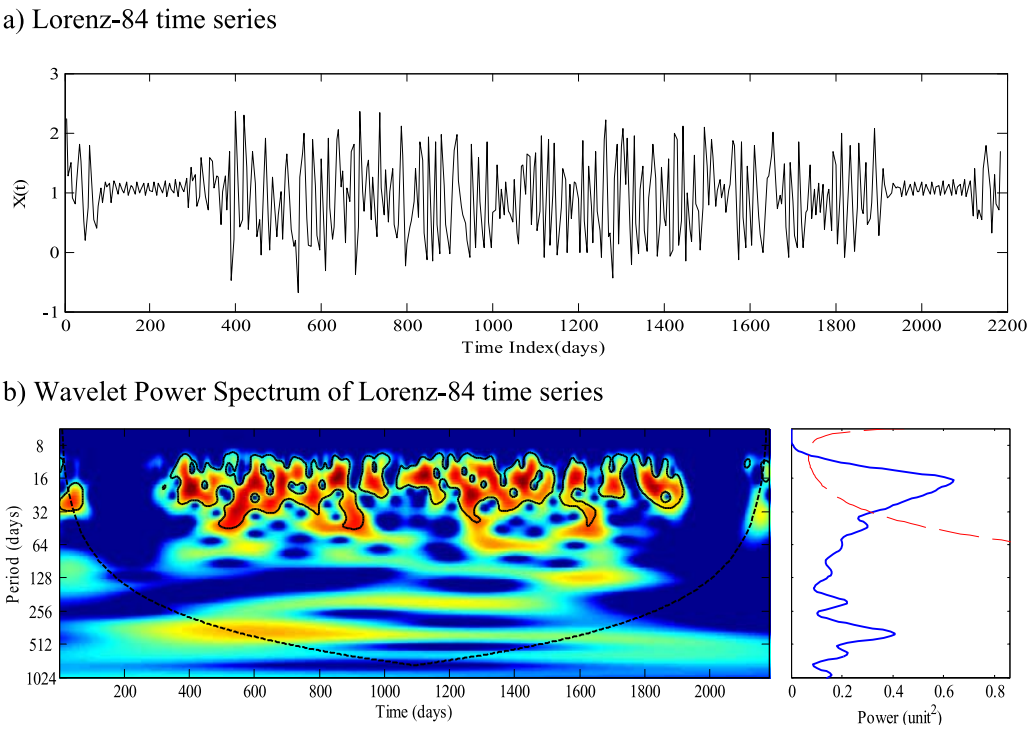

Figure 2. *Lorenz* [1984] **X** variable (a) time series and (b) wavelet power spectrum and the global wavelet power (GWP) spectrum. Black contours in the spectra represent the 95% confidence level compared to red noise. The dashed black line is the cone of influence, where zero padding has reduced the variance. The dashed red line is the significance for the global wavelet spectrum, assuming the same significance level and background spectrum as in wavelet power spectra. All analyses employed the Morlet wavelet.

better than the AR model as well. Note that these frequencies were not included in building WARM since they did not pass the significance test for component selection. From a nonlinear dynamics perspective, the reproduction of trajectory properties in simulations, e.g., Lyapunov exponents that measure predictability, would also be worth checking. However, here our goal is to see

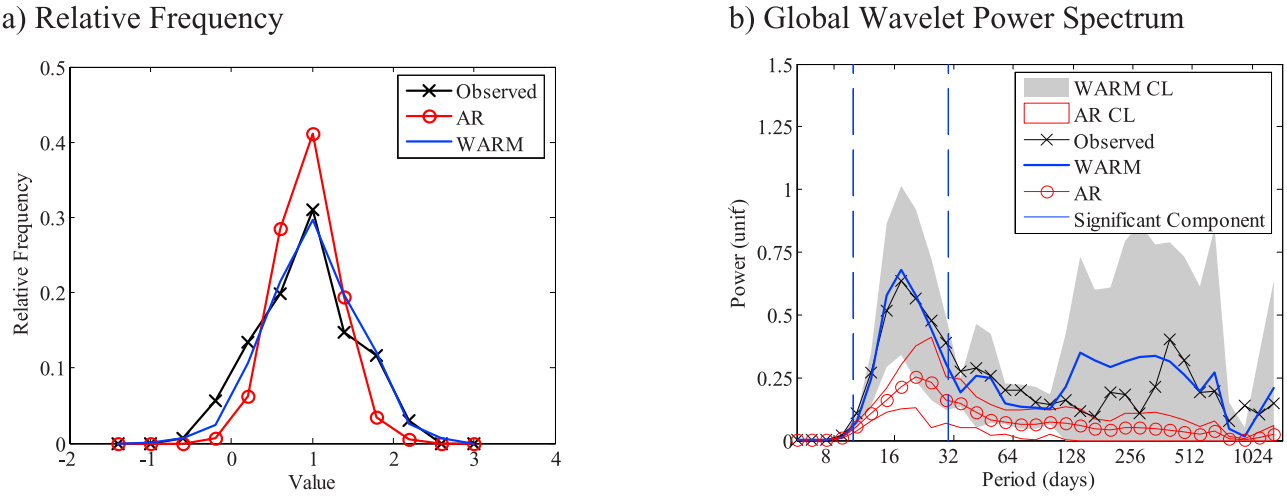

Figure 3. Comparison of (a) average relative frequency distribution and (b) global wavelet power spectrum of 1000 simulations for the Lorenz-84 model using the AR and WARM models. Here $a = 0.25$, $b = 4$, $F_{function}$ and $G = 1$, based on 1000 simulations from each fitted model. The 5th and 95th percentiles of the wavelet spectra from the 1000 WARM and AR simulation are shown. The solid lines represent the average of the spectrum at each frequency across the 1000 simulations. WARM was fitted only using components in the 10–30 day band. The reproduction of the GWP spectrum at the longer periods was not by design.

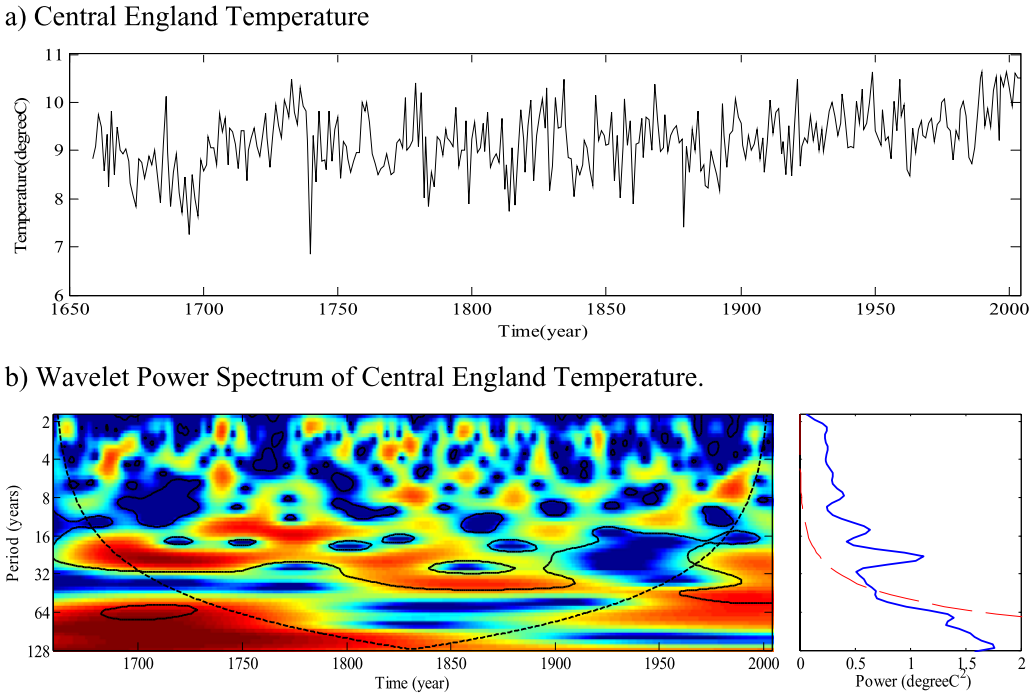

Figure 4. Central England temperature (a) time series and (b) wavelet power spectrum and the global wavelet power (GWP) spectrum. Black contours in the spectra represent the 95% confidence level compared to red noise. The dashed black line is the cone of influence, where zero padding has reduced the variance. The dashed red line is the significance for the global wavelet spectrum, assuming the same significance level and background spectrum as in wavelet power spectra. All analyses employed the Morlet wavelet.

if attributes that have been traditionally a concern for stochastic hydrologists are reproduced better by WARM.

3.2. Annual Central England Temperature

[27] A comparison of AR and WARM models to the record of the annual central England temperature (CET) from 1659 to 2004 is presented in this section. The data were acquired from The Hadley Centre (http://www.met-office.gov.uk/research/hadleycentre/) in England, and represent a historically recorded time series with infilling and bias correction by various methods [*Manley*, 1974; *Parker and Horton*, 2005; *Parker et al.*, 1992]. The CET record has value as one of the longest instrumental temperature records. In recent years, numerous studies have attempted to find and explore CET variability [*Allen et al.*, 1992; *Baliunas et al.*, 1997; *Elsner and Tsonis*, 1991, 1994; *Ghil and Vautard*, 1991; *Plaut et al.*, 1995]. The CET time series (Figure 4a), its Wavelet power spectrum, and the corresponding global wavelet power spectrum of CET are shown in Figure 4b.

[28] We note that the entire 1–32 year band has a GWP level higher than the red noise significance level. The wavelet power spectrums around 64 years and 128 years are comparatively strong but they are not statistically significant using the red noise criteria, and there is evidence of a secular trend. The trend is likely related to the

Table 1. Time Series Descriptions and Specific Attributes for Wavelet Transform Based Simulation

Data Descriptions	Lorenz-84	Central England Temperature	Nino3.4 SST Anomaly	ENP Rainfall		
				FMA	MJJ	ASO
Duration	6 years	1659–2004	1856–2005	1965–2000	1965–2000	1965–2000
δ_t	pentad (5 days)	yearly	monthly	seasonal	seasonal	seasonal
Number of RCs	7	26	13	7	10	9
Significant components	10.3,12.3, 14.6,17.4, 20.6, 24.6, 29.3 day	1.4, 1.6, 1.8, 2.1, 2.4, 2.7, 3.1, 3.6, 4.1, 4.7, 5.5, 6.3, 7.2, 8.3, 9.5, 10.9, 12.5, 14.4, 16.5, 19.0, 21.8, 25.1, 28.8, 33.1 year	1.0, 1.2, 1.4, 1.6, 1.9, 2.3, 2.7, 3.3, 3.9, 4.6, 5.5, 6.5, 7.8 year	1.7, 2.1, 2.5, 2.9, 3.5, 4.1, 4.9 year	1.7, 2.1, 2.5, 2.9, 3.5, 4.1, 4.9, 5.8, 6.9, 8.3 year	1.7, 2.1, 2.5, 2.9, 3.5, 4.1, 4.9, 5.8, 6.9 year
Optimum lags for components	1–3	1–12	3–5	1–3	1–5	1–3
Optimum lag noise	1	2	1	1	2	2

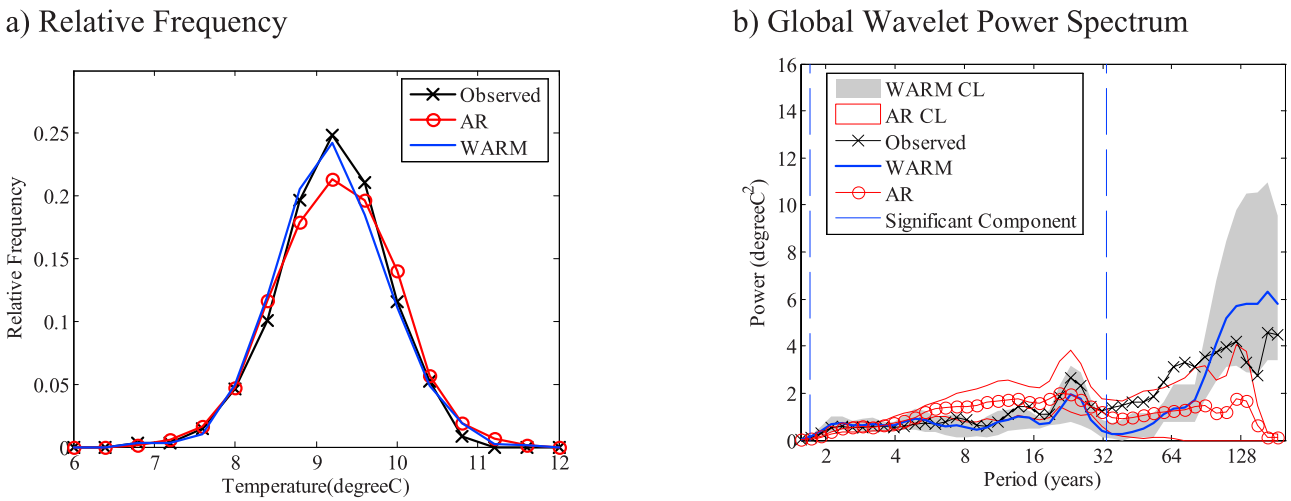

Figure 5. Comparison of (a) average relative frequency distribution and (b) global wavelet power spectrum of 1000 simulations for the central England temperature using the AR and WARM models.

anthropogenic climate change in the 20th century. Here we considered only the 1–32 year band, and used twenty six components for WARM at the frequencies indicated in Table 1. The order of the AR models for these components varied from 1 to 12.

[29] The CET data were transformed to be approximately normally distributed using the Box-Cox transform and then an AR model was applied. The optimal order p of this model was one. Note that since the secular trend was not removed in this data set, it is not meaningful to apply the usual criteria for model selection, or to build an AR model. AR simulations using the Box-Cox transformed data were back transformed to the original space prior to comparisons with WARM simulations or the original data. WARM applications did not consider any prior transformation of the data. One thousand stochastic simulations of each model were then performed.

[30] Figure 5a shows the relative frequency of the simulated time series values. In simulation results, both the AR model and WARM model generally preserve the marginal distribution of the CET data. The comparisons of the global wavelet spectra simulated are shown in Figure 5b. The spectral uncertainties associated with the WARM simulation over all cover the original time series within the 1–32 year frequency band which is the target band for the WARM simulation while the features for periods longer than 32 years, that were not explicitly modeled, are not reproduced. We notice that there are similarities between the AR and WARM and observed spectra in that the dominant peak at around 22 years is reproduced, by both. However, there are substantial differences in the resulting spectra at the higher-frequency end of this band. We suspect that the secular trend in the moments of the CET series influences the response of the fitted AR spectra. Since the variance associated with the components of WARM does not sufficiently exceed the base level in this band, the associated peaks are not reproduced very well. The WARM uncertainty band does generally cover the original spectrum in the 1–32 year band that was used to decompose the original series, while the uncertainty band of the AR simulations is somewhat above the original spectrum over most of this frequency range. The width of the WARM uncertainty band is comparable to the width of the AR uncertainty band over most of the frequency range. The main region over which the uncertainty band for the WARM simulation is much larger is for periods greater than about 100 years, where its amplitude is also much higher.

[31] Another interesting observation is that the AR spectrum tends to be rather flat over the frequency range considered, while the WARM simulations suggest a much sharper peak in the extreme low-frequency end similar to that in the observed spectrum. Given the limited degrees of freedom, it is not useful to speculate too much about these differences. However, it does seem that the WARM approach may be decomposing the secular trend and associated low-frequency changes somewhat better than the AR model where no explicit frequency separation is attempted. We explored this idea by simulating sequences from WARM using only the wavelet components and not including the autoregressive model for the noise term ω_t. The resulting GWP spectrum is similar to the WARM spectrum shown in Figure 5b up to about a period of 64 years, and is considerably lower thereafter, suggesting that the trend components are aliased into the noise term. In an operational setting, as opposed to this exploratory exercise, one would want to address the trend explicitly in both cases, e.g., using an ARIMA model instead of the AR, and by isolating the lowest frequency components as trend in WARM. The latter is particularly interesting since it would allow us to assess the contribution of the trend to the series variance. The scale-averaged wavelet power associated with all frequencies below some cutoff frequency would help assess the temporal variation in the trend and its variance.

3.3. Monthly NINO3.4 SST Index

[32] The monthly Nino3.4 SST anomaly series from 1856 to 2005 (Figure 6a) has been analyzed as a surrogate for ENSO variability that is established from many analyses to be prominent in the 2–8 year band [*Allan et al.*, 1995; *Barnett*, 1991; *Torrence and Compo*, 1998; *Torrence and Webster*, 1999; *Wang and Wang*, 1996]. The wavelet power spectrum and the corresponding global wavelet power spectrum of Nino3.4 SST index are shown in Figure 6b.

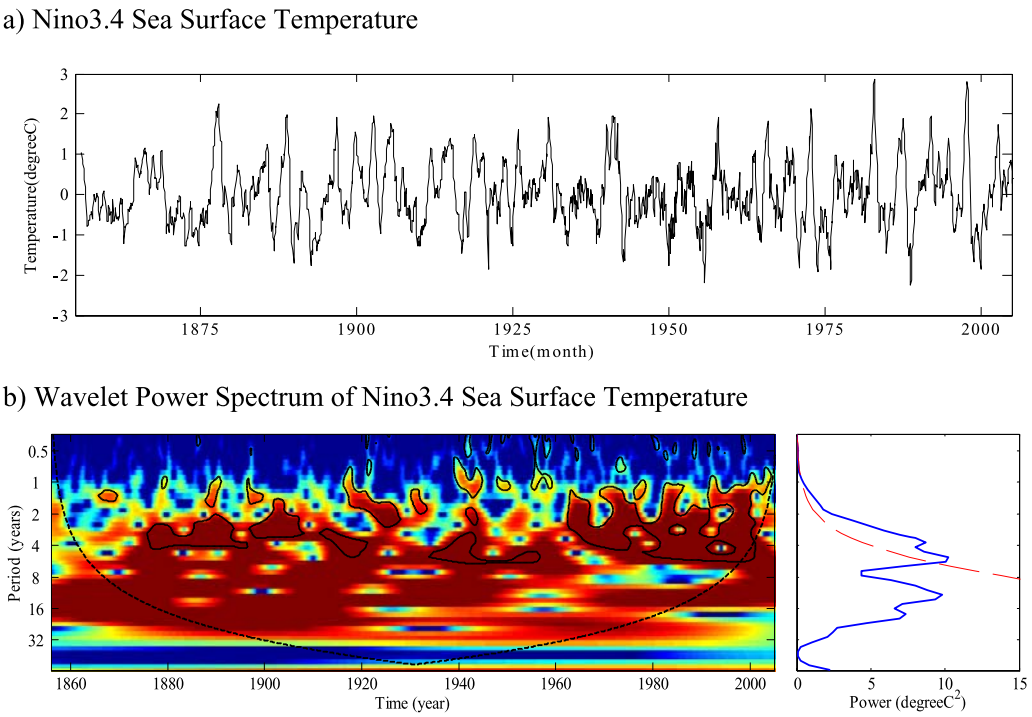

Figure 6. Nino3.4 sea surface temperature (a) time series and (b) wavelet power spectrum and the global wavelet power (GWP) spectrum. Black contours in the spectra represent the 95% confidence level compared to red noise. The dashed black line is the cone of influence, where zero padding has reduced the variance. The dashed red line is the significance for the global wavelet spectrum, assuming the same significance level and background spectrum as in wavelet power spectra. All analyses employed the Morlet wavelet.

The NINO3.4 index is defined through the average of the sea surface temperature (SST) field over the region bounded by 5°N to 5°S, from 170°W to 120°W. The data set was acquired from KNMI (http://www.knmi.nl/). The index is presented as a monthly anomaly series or departure from the mean value.

[33] There is a history of modeling the ENSO (e.g., SOI) series using traditional time series models, and the AR (3) was previously reported as optimal using a data set from 1935 to 1983 [*Chu and Katz*, 1985]. *Trenberth and Hoar* [1996] used an ARMA(3, 1) model for Darwin sea level pressure anomalies for the period from 1882 to 1981. To be consistent with this work, we first used a Box-Cox transform to convert the monthly NINO3.4 data to be approximately normally distributed, and then applied both the AR and the ARMA models with parameter selection as before. The optimal order p selected for the AR model was five, and the (p, q) for the ARMA model were (2, 1). WARM was applied to the untransformed data as before. Following the procedure described earlier, thirteen components were identified for WARM, all within the 1.7 to 8 year frequency band, and the corresponding component AR models had order ranging from three to five.

[34] The comparisons of the marginal distributions of the average from 1,000 simulations are shown in Figure 7a. We note that all methods reproduce the observed frequency distribution similarly. The comparison of the GWP spectra is provided in Figure 7b. On the basis of observational analyses as well as numerical modeling results [*Cane and Zebiak*, 1985; *Ji et al.*, 1996; *Syu et al.*, 1995], ENSO is typically considered to be primarily an interannual phenomenon (2–8 year band) with some discussion of lower-frequency variability. Here we note that the WARM spectrum is better tuned to the observed spectrum than either the AR or the ARMA spectrum. Indeed, the observed spectra is above the uncertainty band for the ARMA (AR is similar) simulations in this band. The ARMA spectra actually appear to be better tuned to the interdecadal variations in the 10–30 year band that were not deemed statistically significant based on the red noise criteria.

[35] From our applications, we notice that AR and ARMA spectra fitted to a series typically smooth across the peaks in the observed spectra, while WARM reproduces the part of the spectra considered significant with respect to red noise, and may generate harmonics or lower-frequency variations depending on the character of the residual noise term. Here WARM does not generate the interdecadal peaks (not statistically significant) in the original spectrum. So the possibilities are (1) these peaks are not harmonics of the components in the 2–8 year band that were modeled and/or (b) they are spurious. The AR and ARMA spectra, on average lie within the WARM uncertainty bands, so we cannot reject them as implausible even if we accepted the WARM to be a better model. Likewise, the average WARM spectrum in the 8–32 year band lies inside the ARMA uncertainty band, which in this case is much wider than the WARM uncertainty band over the same frequency range. So, if we go by the red noise selection criteria, WARM has a lower bias and higher uncertainty near the peak of the original spectrum that was deemed statistically significant,

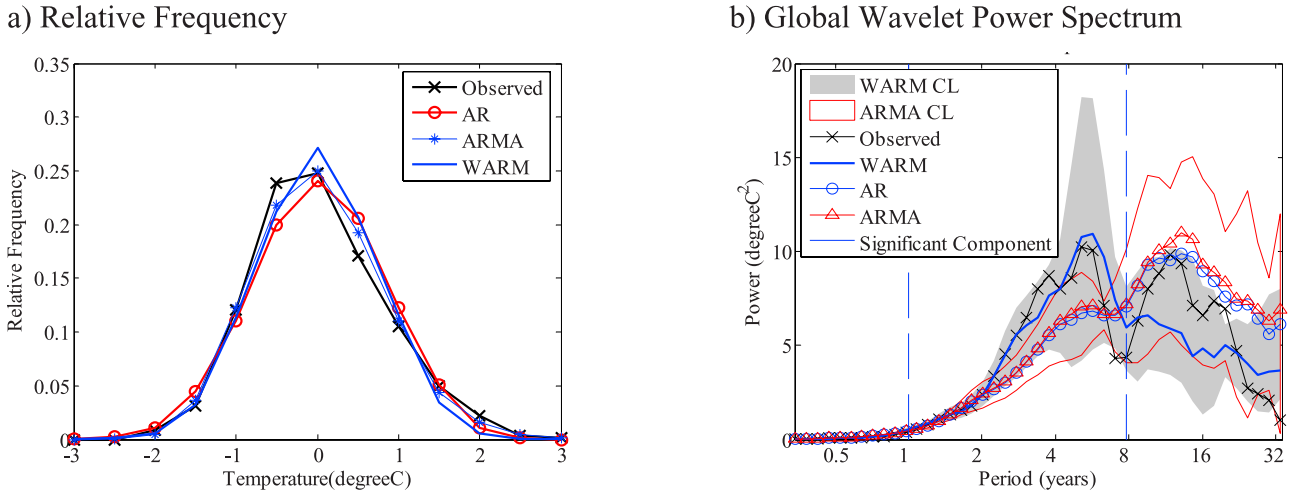

Figure 7. Comparison of (a) average relative frequency distribution and (b) global wavelet power spectrum of 1000 simulations for the Nino3.4 Sea surface temperature using the AR, ARMA, and WARM models.

while ARMA has a lower bias but higher variance in the broad band frequency range from 8 to 32 years. A systematic comparison of these differences considering parameter and model uncertainty in fitting the models and drawing samples not just from the historical data, but also from physically based ENSO models may help highlight whether the differences are meaningful or spurious.

3.4. Everglades Seasonal Rainfall

[36] The long-term simulation of the rainfall in the Everglades National Park (ENP) was the original motivation for our work. The ENP rainfall data exhibits quasi-oscillatory behavior that may derive from low-frequency Pacific and Atlantic Ocean climate modes. The connection of these low-frequency climate modes to Lake Okeechobee inflows and southern Florida rainfall has been noted by *Enfield et al.* [2001], *Kwon et al.* [2006], *Miralles-Wilhelm et al.* [2005], *Schmidt et al.* [2001], and *Trimble et al.* [1998]. The sign and strength of the correlation of the Everglades rainfall to the NINO3.4 index is seasonally variable. Consequently, we wanted to explore how interannual variations in the rainfall for specific seasons could be best modeled and simulated. An ENP rainfall index was computed by averaging the rainfall data at eight local rain gauges located in and around the southern Everglades region for which reliable long-term data are readily available. Figure 8 shows the map with the network of the selected rain gages.

[37] The period of record of rainfall data analyzed here extends from 1965 to 2000. Seasonal data were derived from the 1965–2000 monthly rainfall record. The main rainy season extends from mid-May to October. Consequently, three seasons were considered: February-March-April (FMA); May-June-July (MJJ); and August-September-October (ASO).

[38] The first step in assessing seasonal variability is to apply the wavelet transform to each of the seasonal rainfall. Figure 9 shows the wavelet power spectrum and its corresponding global wavelet power spectrum for annual rainfall, FMA, MJJ and ASO seasonal rainfall. A broad peak with a period of 2–8 years is evident in the wavelet power spectrum and global power spectrum in most of the seasons, indicating the presence of the interannual variation throughout the last several years. The FMA and ASO season also indicate interdecadal variation in the last thirty years but these spectra are not statistically significant relative to the red noise confidence limits.

[39] Each season's rainfall series was modeled separately using WARM as an annual time series. The number of components selected was seven, ten and nine for the three seasons, respectively. The optimal lag orders of these components were found to vary between one and five. A periodic AR (PAR) model is used to consider seasonality of rainfall. The PAR model is defined as [*Salas et al.*, 1980]:

$$x_{m,t} = \sum_{j=1}^{p_m} \alpha_{j,m} x_{m-j,t} + \varepsilon_{m,t} \quad m = 1, \ldots, n_{season} \quad t = Year\ index \tag{10}$$

where $x_{m,t}$ is the seasonal rainfall time series for season m, in year t, $\alpha_{j,m}$ are autoregressive coefficients, $\varepsilon_{m,t}$ is a noise process and $n_{season} = 4$.

[40] For the reference PAR model, the raw rainfall data was once again transformed to be approximately normal using the Box-Cox transform, and the order selected by AIC for all seasons was one. The frequency distribution characteristics calculated from 1000 simulations are compared with those for the historical record in Figures 10a, 10c, and 10e.

[41] The relative frequency comparison in Figure 10 shows that the historical rainfall distributions are reproduced by the simulations based on WARM about as well as by the AR model. However, as in the earlier examples, the WARM simulations are considerably better at reproducing the spectral signatures in the original observations (Figures 10b, 10d, and 10f). Note that in this set of examples, WARM directly models the interannual process for each season without looking at season to season dependence, while the PAR only models the intra-annual process. WARM chooses components in the 2–5 year band for FMA, and in the 2–8 year band for the MJJ and ASO

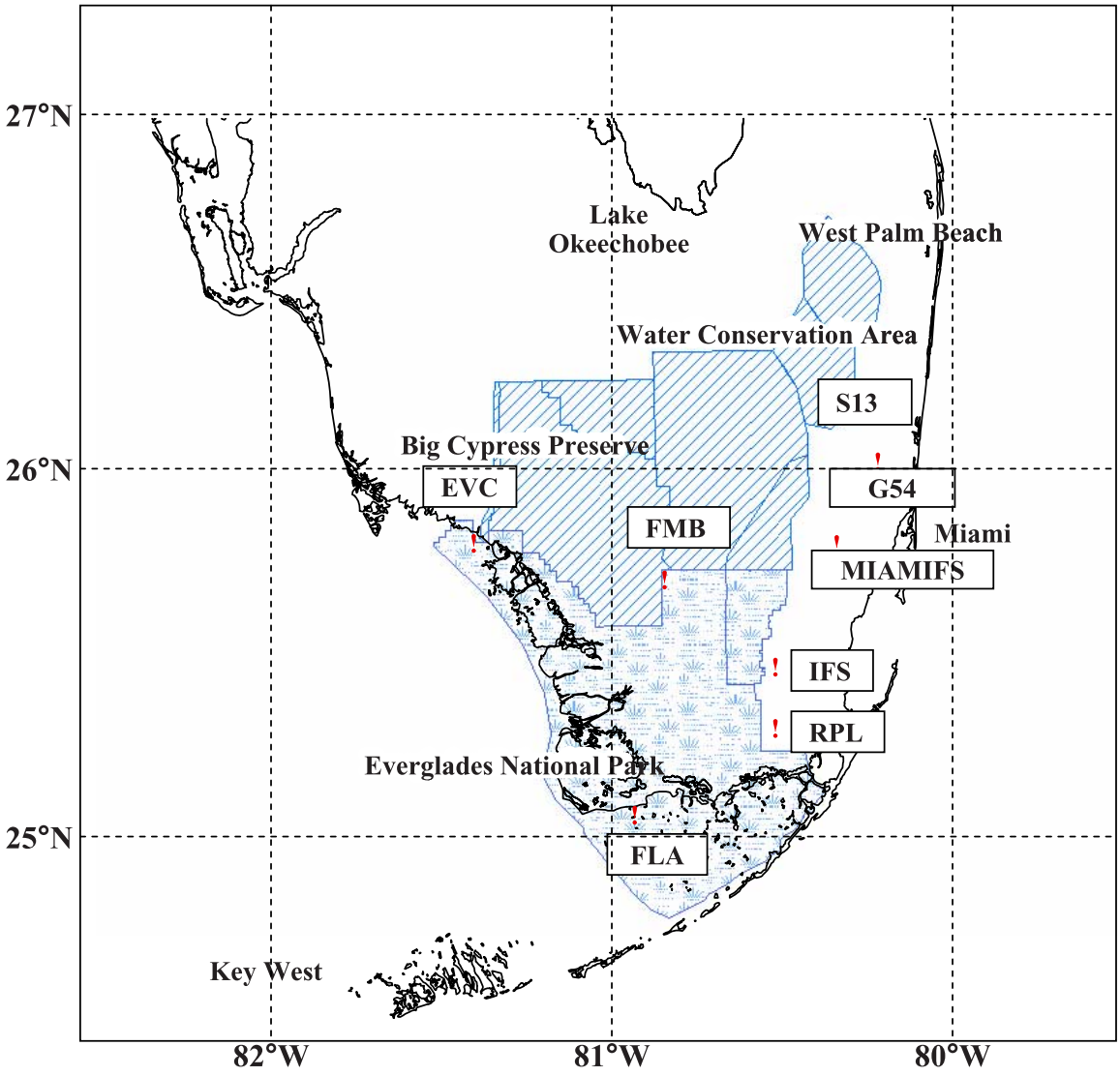

Figure 8. Everglades National Park region and eight weather stations. Boxes indicate main rainfall gauge stations.

seasons. The relatively sharp peak in the observed FMA spectrum around 4 years is better reproduced by WARM than by PAR. However, PAR does generate a broad spectrum over the entire low-frequency band that lies inside the uncertainty band of the WARM simulations. However, the FMA peaks of the observed spectrum are outside the uncertainty band of the PAR simulations. ENSO teleconnections in this frequency band to the ENP rainfall have been previously documented [*Schmidt et al.*, 2001] so the better reproduction of the ENSO signature in this band by WARM relative to AR is useful. The situation is similar for the MJJ and ASO seasons. For these seasons, the WARM simulations bracket the sharp peaks around periods of 3 and 7 years and follow the observed spectrum with some biases. For ASO, a likely spurious peak in the observed spectrum about a 14–16 year period is reproduced by the WARM simulations, suggesting that if it were real, it could be a harmonic of the higher-frequency phenomena, as in the CET case. However, given 35 years of data, it is not useful to compare spectral responses at this frequency. Remarkably, the uncertainty bands associated with the AR simulations are broader over much of the frequency range than those for the WARM simulations.

4. Discussion

[42] It is often said that time series analysis is an art. This statement reflects the inherent subjectivity in such an enterprise if one thinks about the problem. Assumptions are made as to the underlying distributions, model structure (e.g., linearity), and also as to the best criteria to choose model parameters with. Some of these assumptions can and are usually tested with a given data set. Others, such as the performance criteria used for model selection are not. Ideally, a model selected should reproduce behavior of interest across a broad set of metrics (e.g., predictive risk or mean square error, spectrum, spell distributions, extreme events etc.). Consequently, the application of a time series model to data is necessarily an exploratory activity, in addition to the obvious solution of specific estimation problems. Given this context, this paper was motivated by a simple question:

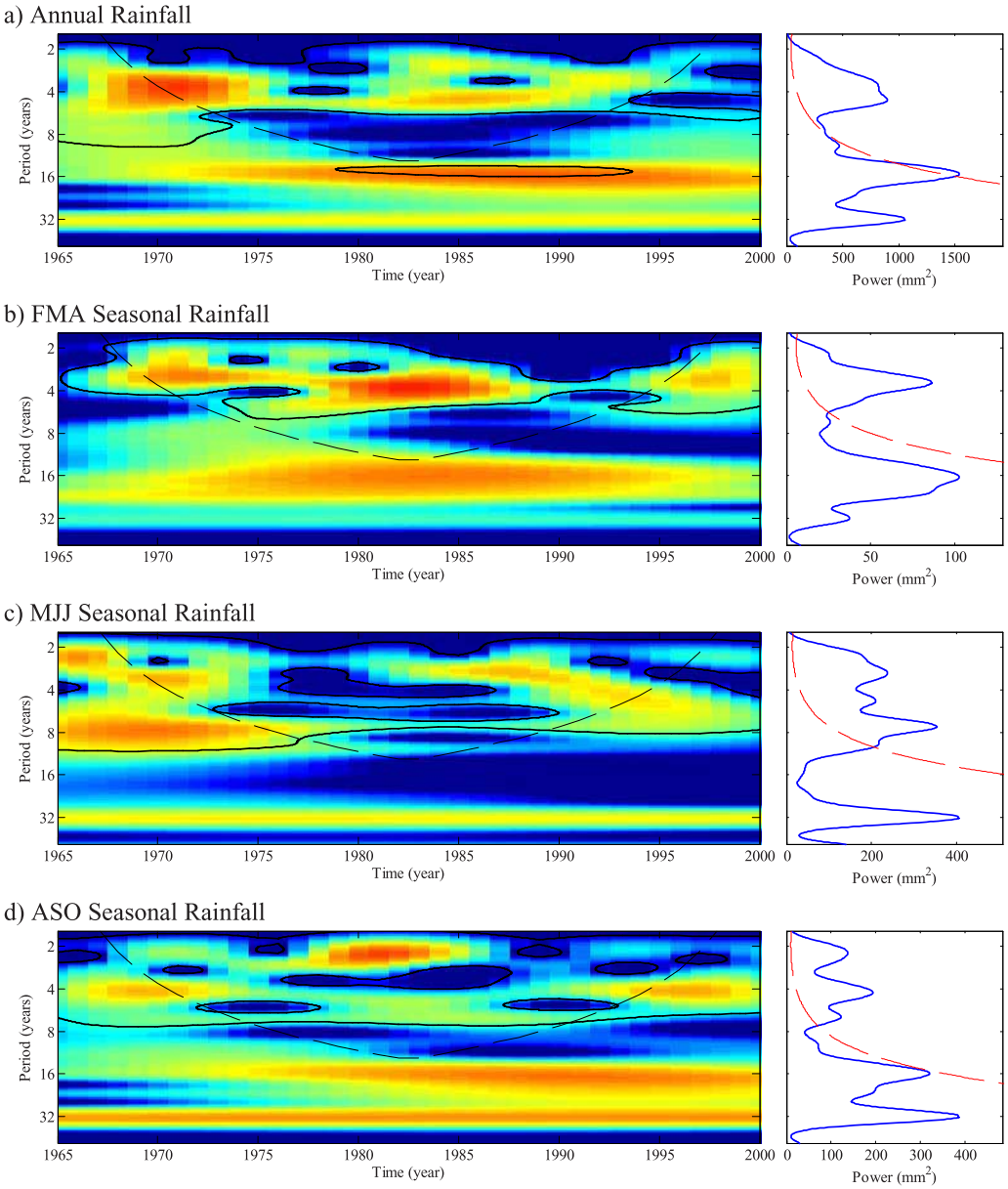

Figure 9. Wavelet analysis of spatially averaged annual and seasonal rainfall in the ENP region. Plots show (left) wavelet power spectra and (right) global average wavelet power for (a) annual and (b–d) the seasonal rainfall (FMA, MJJ, and ASO seasons, respectively).

[43] Could the nonnormality and low-frequency memory observed in hydroclimatic time series be effectively modeled by an approach that decomposes the time series into significant spectral components and noise and then models each such process using a traditional AR process?

[44] To address this question empirically, we considered four examples, and compared the application of one or more of AR, PAR, and ARMA models with WARM. Note that we did not seek to fit the best possible time series model in any of these examples. We focus on specific attributes, accept that the model posed is inadequate in some regard and look for lessons that could be learned under such misclassification. Here we summarize the key observations.

[45] 1. The WARM model generally preserves the marginal distribution of the time series and the lower-order statistics (Figure 11). AR simulations without transformation to normality lead to a significantly biased marginal distribution for the state variable, while WARM reproduces the distribution for the cases analyzed here, suggesting that the mixing properties of the wavelet components and the residual term, each of which was assumed to be normally distributed, may lead to the proper marginal distribution (basis is Lorenz 84 data).

[46] 2. WARM usually reproduces the observed spectrum over the frequency band of fitting, while the AR model does not. The mean AR simulated spectrum is often outside the WARM spectrum uncertainty bounds, suggesting that there

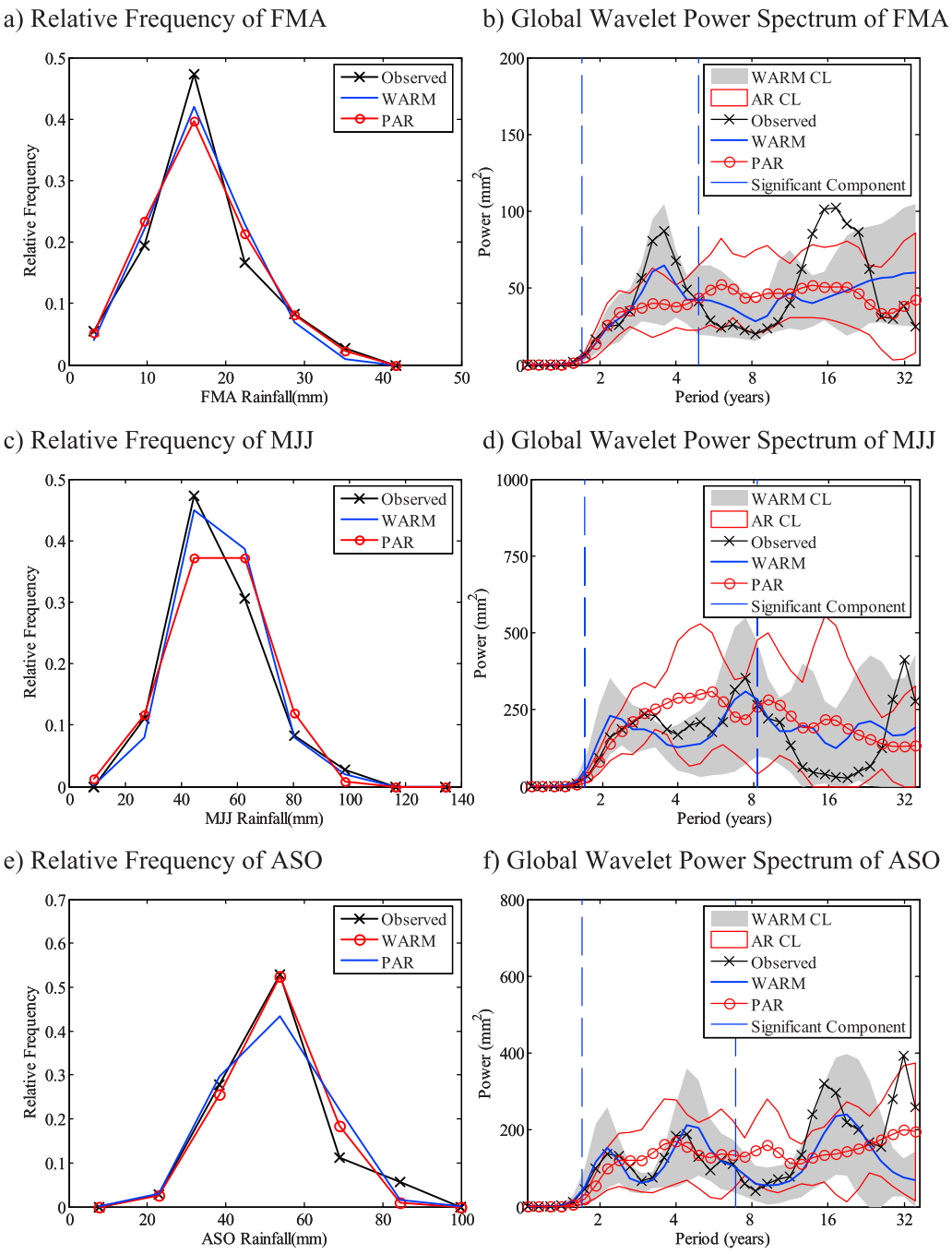

Figure 10. Comparison of relative frequency and global wavelet power spectrum of each simulated seasonal rainfall between PAR model and WARM model (1000 simulations). Relative frequency with (a) FMA seasonal rainfall, (c) MJJ seasonal rainfall, and (e) ASO seasonal rainfall and global wavelet power spectrum (b) FMA seasonal rainfall, (d) MJJ seasonal rainfall, and (f) ASO seasonal rainfall.

is a statistically significant difference between simulations from these two models. The AR, ARMA, and PAR simulated spectra typically do have low-frequency components but are generally broad band instead of being sharp as in the WARM case. Thus, if the underlying phenomena did not correspond to multiple oscillatory modes or regime transitions, then WARM would have a tendency to "overfit" the realization that was observed (basis is NINO3.4 and ENP data sets).

[47] 3. In the presence of monotonic trends as opposed to quasi-oscillatory variability, the direct application of both WARM and AR models as formulated here is likely suspect. For WARM, spurious frequency components whose variance is elevated relative to the red noise criteria may be fit and reproduced. For the AR models, the spectrum is

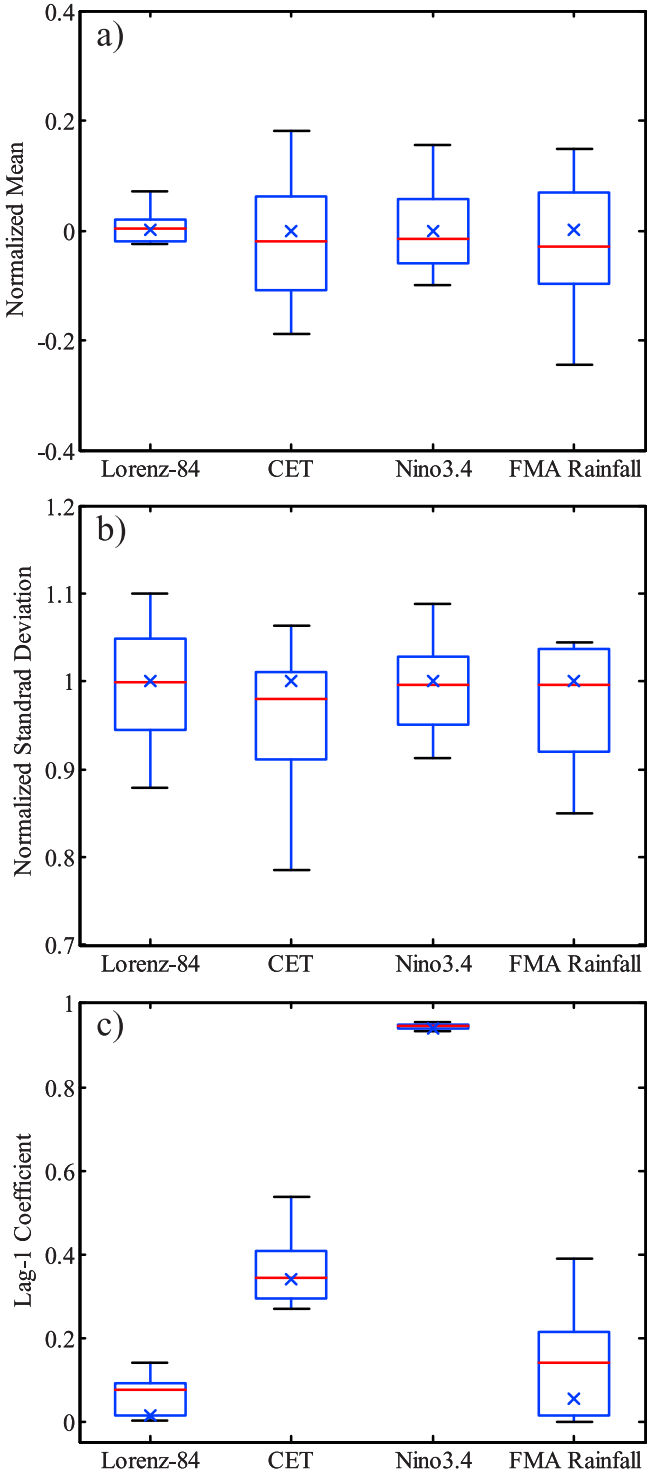

Figure 11. Box plots of (a) the mean, (b) standard deviation, and (c) lag 1 coefficient from the WARM simulations. Crosses indicate the observed statistics.

significantly biased since there is an attempt to also fit the trend (basis is CET data).

[48] 4. It is possible that the data modeled may represent phenomena with a primary oscillatory frequency with higher and/or lower harmonics of that frequency. Neither method as presented explicitly attempts to account for such phenomena. However, the application of both methods may provide some potential for speculation of this nature. For instance, if only a certain set of frequency components in WARM are explicitly fit, and the simulated spectrum as well as the observed spectrum exhibit a strong peak at a harmonic of the fitted frequency, then there is a suggestion that harmonics are present. Since each component is orthogonal and is modeled independently in WARM, interactions across frequency phenomena are not directly considered.

[49] 5. WARM uses considerably more parameters (explicit and implicit) than a traditional Box-Jenkins model. However, each such simulation is expected to and does reproduce the persistence, and oscillatory character of the observed time series. The ARMA model based simulations capture the broad low-frequency spectral distribution of the underlying data on average, but individual simulations do not generally correspond to the spectral/frequency structure of the observations. Where this structure is anticipated, such models will be a poor choice. If the underlying system has longer memory than can be modeled by an ARMA due to nonlinear regime transitions or other factors, then the actual uncertainty associated with the model will be considerably higher than the uncertainty estimated as part of the usual parameter estimation process; that is, AR order and parameter estimates from different segments of the record could be much more different than would be expected for samples of that segment length for a stationary phenomenon. In this case, an alternative would be to develop state-space or hidden Markov models and explore whether they capture the nonhomogeneity or nonstationarity of the underlying process better than WARM.

[50] 6. Given the high number of parameters, and multiple ad hoc rules for selection of components, are WARM models practical and robustly identifiable from the data? This question was not explored here but is an important issue. The "best" approach for model fitting and uncertainty analysis was not the focus of this exploratory study. Future research needs to address how the best frequency components can be identified and the resulting model tested in terms of its performance on a suite of measures, including stochastic Lyapunov exponents, AIC like measures, and closeness to the interesting/plausible aspects of the observed spectrum.

[51] 7. Finally, we observe that for hydroclimatic risk management, an improved assessment of time series attributes such as regime like behavior, quasiperiodic behavior and clustering of events is being increasingly recognized as important, even as questions of anthropogenic climate change, and the potentially monotonic trends that may result from it, are discussed. In this context, the performance of models that "predict" future changes needs to be done in a statistical context. This context includes how the basic statistics of a state variable are reproduced in control simulations, as well as the temporal structure associated with these state variables. The direction of research advanced here would be useful in addressing how well model simulations of ENSO and other quasiperiodic phenomena and their associated hydroclimatic teleconnections are captured by these models. Such investigations would have direct applicability to the analysis of reservoir storage, particularly with respect to system resilience under a par-

ticular water allocation policy, e.g., in the Colorado River Basin.

[52] **Acknowledgments.** Support of this work by the "Climate and Weather Scenario Driven Strategies for the Adaptive Management of ENP Operations to Achieve Hydrologic and Ecologic Restoration Targets" agreement H5297-05-0071 is acknowledged.

References

Abarbanel, H. D. I. (1996), *Analysis of Observed Chaotic Data*, Springer, New York.

Abarbanel, H. D. I., and U. Lall (1996), Nonlinear dynamics of the Great Salt Lake: System identification and prediction, *Clim. Dyn.*, *12*, 287–297.

Ahn, J. H., and H. S. Kim (2005), Nonlinear modeling of El Nino/Southern Oscillation index, *J. Hydrol. Eng.*, *10*, 8–15.

Akaike, H. (1974), New look at statistical-model identification, *IEEE Trans. Automat. Control*, *19*, 716–723.

Allan, R. J., et al. (1995), Multidecadal variability in the climate system over the Indian-Ocean region during the austral summer, *J. Clim.*, *8*, 1853–1873.

Allen, M. R., et al. (1992), Temperature oscillations, *Nature*, *359*, 679.

Baliunas, S., et al. (1997), Time scales and trends in the central England temperature data (1659–1990): A wavelet analysis, *Geophys. Res. Lett.*, *24*, 1351–1354.

Barnett, T. P. (1991), The interaction of multiple time scales in the tropical climate system, *J. Clim.*, *4*, 269–285.

Box, G. E. P., and G. Jenkins (1970), *Time Series Analysis, Forecasting and Control*, Holden-Day, Boca Raton, Fla.

Cane, M. A., and S. E. Zebiak (1985), A theory for El-Nino and the Southern Oscillation, *Science*, *228*, 1085–1087.

Chu, P. S., and R. W. Katz (1985), Modeling and forecasting the Southern Oscillation—A time domain approach, *Mon. Weather Rev.*, *113*, 1876–1888.

Chui, C. K. (1992), *An Introduction to Wavelets: Wavelet Analysis and Its Application* vol. 1, 266 pp., Elsevier, New York.

Dettinger, M. D., et al. (1995), Interannual and interdecadal variability in United-States surface-air temperatures, 1910–87, *Clim. Change*, *31*, 35–66.

Elsner, J. B., and A. A. Tsonis (1991), Do bidecadal oscillations exist in the global temperature record, *Nature*, *353*, 551–553.

Elsner, J. B., and A. A. Tsonis (1994), Low-frequency oscillation, *Nature*, *372*, 507–508.

Enfield, D. B., et al. (2001), The Atlantic multidecadal oscillation and its relation to rainfall and river flows in the continental US, *Geophys. Res. Lett.*, *28*, 2077–2080.

Farge, M. (1992), Wavelet transforms and their applications to turbulence, *Annu. Rev. Fluid Mech.*, *24*, 395–457.

Foufoula-Georgiou, E., and P. Kumar (1995), *Wavelets in Geophysics*, 373 pp., Elsevier, New York.

Ghil, M., and R. Vautard (1991), Interdecadal oscillations and the warming trend in global temperature time-series, *Nature*, *350*, 324–327.

Huang, Z., and Z. S. Chalabi (1995), Use of time-series analysis to model and forecast wind-speed, *J. Wind Eng. Ind. Aerodyn.*, *56*, 311–322.

Hubbard, B. B. (1996), *The World According to Wavelets: The Story of a Mathematical Technique in the Making*, 286 pp., A. K. Peters, Wellesley, Mass.

Hughes, J. P., and P. Guttorp (1999), A non-homogeneous hidden Markov model for precipitation occurrence, *J. R. Stat. Soc., Ser. C*, *48*, 15–30.

Jain, S. (1998), Low-frequency climate variability: Inferences from simple models, Ph.D. thesis, 187 pp., Dep. of Civ. and Environ. Eng., Utah State Univ., Logan.

Jain, S., et al. (1999), Seasonality and interannual variations of Northern Hemisphere temperature: Equator-to-pole gradient and ocean-land contrast, *J. Clim.*, *12*, 1086–1100.

Ji, M., et al. (1996), Coupled model predictions of ENSO during the 1980s and the 1990s at the National Centers for Environmental Prediction, *J. Clim.*, *9*, 3105–3120.

Jiang, N., et al. (1995), Quasi-quadrennial and quasi-biennial variability in the equatorial Pacific, *Clim. Dyn.*, *12*, 101–112.

Kaiser, G. (1994), *A Friendly Guide to Wavelets*, 300 pp., Birkhäuser, Boston, Mass.

Kennel, M. B., and A. I. Mees (2000), Testing for general dynamical stationarity with a symbolic data compression technique, *Phys. Rev. E*, *61*, 2563–2568.

Kennel, M. B., et al. (1992), Determining embedding dimension for phase-space reconstruction using a geometrical construction, *Phys. Rev. A*, *45*, 3403–3411.

Keppenne, C. L., and M. Ghil (1992a), Adaptive filtering and prediction of the Southern Oscillation index, *J. Geophys. Res.*, *97*, 20,449–20,454.

Keppenne, C. L., and M. Ghil (1992b), Extreme weather events, *Nature*, *358*, 547.

Keppenne, C. L., and U. Lall (1996), Complex singular spectrum analysis and multivariate adaptive regression splines applied to forecasting the Southern Oscillation, *Exp. Long Lead Forecast Bull.*, *5*, 54–56.

Koutsoyiannis, D. (1994), A stochastic disaggregation method for design storm and flood synthesis, *J. Hydrol.*, *156*, 193–225.

Kulkarni, J. R. (2000), Wavelet analysis of the association between the Southern Oscillation and the Indian summer monsoon, *Int. J. Climatol.*, *20*, 89–104.

Kwon, H.-H., et al. (2006), Episodic interannual climate oscillations and their influence on seasonal rainfall in the Everglades National Park, *Water Resour. Res.*, *42*, W11404, doi:10.1029/2006WR005017.

Lall, U., and M. Mann (1995), The Great Salt Lake: A barometer of low-frequency climatic variability, *Water. Resour. Res.*, *31*, 2503–2515.

Lall, U., and A. Sharma (1996), A nearest neighbor bootstrap for resampling hydrologic time series, *Water. Resour. Res.*, *32*, 679–693.

Lorenz, E. N. (1984), Irregularity: A fundamental property of the atmosphere, *Tellus, Ser. A*, *36*, 98–110.

Lorenz, E. N. (1990), Can chaos and intransitivity lead to interannual variability?, *Tellus, Ser. A*, *42*, 378–389.

Manley, G. (1974), Central England temperatures—Monthly means 1659 to 1973, *Q. J. R. Meteorol. Soc.*, *100*, 389–405.

Mann, M. E., and J. Park (1993), Spatial correlations of interdecadal variation in global surface temperatures, *Geophys. Res. Lett.*, *20*, 1055–1058.

Mann, M. E., and J. Park (1994), Global-scale modes of surface-temperature variability on interannual to century timescales, *J. Geophys. Res.*, *99*, 25,819–25,833.

Mann, M. E., and J. Park (1996), Joint spatiotemporal modes of surface temperature and sea level pressure variability in the Northern Hemisphere during the last century, *J. Clim.*, *9*, 2137–2162.

Miralles-Wilhelm, F., et al. (2005), Climate-based estimation of hydrologic inflow into Lake Okeechobee, Florida, *J. Water Res. Plann.*, *131*, 394–401.

Parker, D., and B. Horton (2005), Uncertainties in central England temperature 1878–2003 and some improvements to the maximum and minimum series, *Int. J. Climatol.*, *25*, 1173–1188.

Parker, D. E., et al. (1992), A new daily central England temperature series, 1772–1991, *Int. J. Climatol.*, *12*, 317–342.

Plaut, G., et al. (1995), Interannual and interdecadal variability in 335 years of central England temperatures, *Science*, *268*, 710–713.

Rajagopalan, B., et al. (1998), A multivariate frequency-domain approach to long-lead climatic forecasting, *Weather Forecast*, *13*, 58–74.

Robertson, A. W., et al. (2004), Downscaling of daily rainfall occurrence over northeast Brazil using a hidden Markov model, *J. Clim.*, *17*, 4407–4424.

Roebber, P. J. (1995), Climate variability in a low-order coupled atmosphere-ocean model, *Tellus, Ser. A*, *47*, 473–494.

Salas, J. D., et al. (1980), *Applied Modelling of Hydrologie Time Series*, Water Resour. Publ., Highlands Ranch, Colo.

Schmidt, N., et al. (2001), ENSO influences on seasonal rainfall and river discharge in Florida, *J. Clim.*, *14*, 615–628.

Stedinger, J. R., and R. M. Vogel (1984), Disaggregation procedures for generating serially correlated flow vectors, *Water Resour. Res.*, *20*, 47–56.

Syu, H. H., et al. (1995), Seasonal and interannual variability in a hybrid coupled GCM, *J. Clim.*, *8*, 2121–2143.

Thomas, H. A., and M. B. Fiering (1962), Mathematic synthesis of streamflow sequences for analysis of river basins by simulation., in *Design of Water Resources Systems*, edited by A. Mass, pp. 459–493, Harvard Univ. Press, Cambridge, Mass.

Tong, H. (1990), *Non-linear Time Series: A Dynamical System Approach*, Clarendon, Oxford, U. K.

Torrence, C., and G. P. Compo (1998), A practical guide to wavelet analysis, *Bull. Am. Meteorol. Soc.*, *79*, 61–78.

Torrence, C., and P. J. Webster (1999), Interdecadal changes in the ENSO-monsoon system, *J. Clim.*, *12*, 2679–2690.

Trenberth, K. E., and T. J. Hoar (1996), The 1990–1995 El Nino Southern Oscillation event: Longest on record, *Geophys. Res. Lett.*, *23*, 57–60.

Trimble, P. J., et al. (1998), A refined approach to Lake Okeechobee water management: An application of climate forecast, special report, 73 pp., South Fla. Water Manage. Dist., West Palm Beach.

Valencia, D., and J. C. Schaake (1973), Disaggregation Processes in stochastic hydrology, *Water Resour. Res.*, *9*, 580–585.

Wang, B., and Y. Wang (1996), Temporal structure of the Southern Oscillation as revealed by waveform and wavelet analysis, *J. Clim.*, *9*, 1586–1598.

Weng, H. Y., and K. M. Lau (1994), Wavelets, period-doubling, and time-frequency localization with application to organization of convection over the tropical western Pacific, *J. Atmos. Sci.*, *51*, 2523–2541.

Yevjevich, V. (1972), *Stochastic Processes in Hydrology*, Water Resour. Publ., Highlands Ranch, Colo.

A. F. Khalil, H.-H. Kwon, and U. Lall, Department of Earth and Environmental Engineering, Columbia University, New York, NY 10027, USA. (hk2273@columbia.edu)